Visual simulation of bone cement blending and dynamic flow

1st Long Shen
School of Intelligence Science and Technology, University of Science and Technology Beijing
Beijing, China
sl_111211@163.com

2nd Yalan Zhang*
School of Intelligence Science and Technology, University of Science and Technology Beijing
Beijing, China
zhangyl@ustb.edu.cn

3rd Steffen Frey
Bernoulli Institute University of Groningen
Groningen, the Netherlands
s.d.frey@rug.nl

4th Alex Telea
Department of Information and Computing Sciences Utrecht University
Utrecht, the Netherlands
a.c.telea@uu.nl

5th Jiří Kosinka
Bernoulli Institute University of Groningen
Groningen, the Netherlands
j.kosinka@rug.nl

6th Xiaokun Wang
School of Intelligence Science and Technology, University of Science and Technology Beijing
Beijing, China
wangxiaokun@ustb.edu.cn

7th Xiaojuan Ban*
Beijing Key Laboratory of Knowledge Engineeringfor Materials Science, University of Science and Technology Beijing
Beijing, China
banxj@ustb.edu.cn

***Abstract*—Bone cement filling is an important method for preventing osteoporosis and treating fractures. In bone cement filling surgery, the preparation and dosage of the cement usually depend on specific product manuals and the doctor's experience. If bone cement is not used properly, it may cause additional damage. For teaching and auxiliary medical purposes, for example, assisting doctors to observe the possible flow of bone cement, this paper proposes a multiphase non-Newtonian fluid simulation method to simulate and visualize the flow behavior during the wet sand phase of bone cement blending and polymerization. Our method enables showing intuitively the application process of bone cement under different scene settings to obtain dynamic bone cement effects with high stability and performance. Compared with other methods, our method can simulate highly viscous mixed fluids efficiently and robustly, which supports our method's usage in the aforementioned training and experimentation scenarios.**

***Index Terms*—Medical visualization, Bone filling simulation, Multiphase non-Newtonian fluid modeling, Bone cement effects**

I. Introduction

With the rising life expectancy and an aging population, about 200 million people worldwide suffer from osteoporosis, fractures and other diseases that can occur at any time. Bone cement filling is an early intervention in osteoporosis and also an important treatment option for bone fractures [1], [2].

In the process of using bone cement, medical doctors usually need to carefully mix it according to their own experience and specific product instructions to prevent bone cement leakage or insufficient dispersion (Fig. 1). This trial-and-error process can be time- and effort-intensive and is not conducive to low-cost teaching. Computer simulation and visualization techniques can help, at a low cost, doctors intuitively understand different preparation scenarios and the impact of the operation on the surgical results.

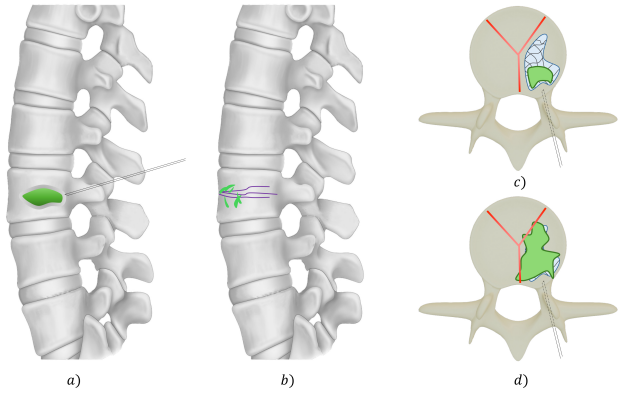

Fig. 1. *a*) Schematic diagram of bone cement (green) filled inside a bone (gray). *b*) When there is a fracture(as shown by purple lines), and the cement is too thin, the pressure inside the bone and a low modulation ratio may cause the cement to leak from the fracture. *c*) If the cement is too thick, it may cause obstruction, and the bone cannot be fully filled. *d*) When the cement is diffused inside the bone, it may reach the nerve (red) and cause complications.

Current research on the simulation and visualization of highly viscous mixed fluids, such as cement, is limited. To address this problem, we propose a new multiphase non-Newtonian fluid simulation method for bone cement preparation and coarse sand flow, which is the early stage of the bone cement flow state. Our contributions are:

- a viscoelastic stress method based on an implicit mixture model and conformation tensor;
- a unified framework for describing Newtonian and non-Newtonian fluids;
- a bonding effect network for controlling the implicit

Fig. 2. Structural support in vertebral augmentation. Left: Deformed vertebrae caused by damage or osteoporosis. Right: Bone cement filling (green) can effectively restore the original structure.

mixture model's phase transfer.

Our model allows physicians to quickly set up Newtonian or non-Newtonian fluids with different properties and perform simulation of mixing, injection, etc. This in turn allows specialists to quickly investigate various scenarios and parameter settings (for the bone cement mix) and also helps with training.

We start by reviewing relevant related work (Section II), then present our simulation method (Section III), describe our experiments and results (Section IV), and finally conclude the paper (Section V).

II. Related Work

A. Bone cement filling

Bone cement filling is an important method for orthopedic joint replacement and the treatment of osteoporosis. In the 1960s, Charnley [3] was the first to apply polymethyl methacrylate (PMMA) to the fixation of femoral prosthesis and acetabulum. More bone cement materials have been extensively investigated in dentistry since the 1970s such as polyzinc carboxylate [4] and glass polylinoate cement [5], [6].

With the advancement of minimally invasive surgical techniques, vertebral augmentation [7], [8] has become the most commonly used surgical procedure for treating osteoporotic compression fractures. By injecting bone cement, the damaged bone can be preserved in its original form. During the process of vertebral augmentation, bone cement is injected as a filler into the damaged bone to maintain its morphology (Fig. 2). However, when using bone cement, strict operating procedures are required to reduce the risk of postoperative complications. Improper operation can cause bone cement leakage; a large amount of leakage can lead to fatal consequences such as pulmonary embolism and paraplegia [9], [10].

B. Physics-based simulation methods

Given the expenses incurred with running multiple physical experiments to assess how bone cement will behave in a concrete given context (that is, bone morphology), *physics-based simulations* are an attractive alternative both for professionals and, potentially even more importantly, for training practitioners. We outline below related work in fluid simulations which is relevant to our context.

Smoothed Particle Hydrodynamics (SPH): The SPH method [11] uses particles to sample the fluid and calculate its physical properties during a simulation. SPH has high numerical accuracy and can capture details such as the splash of droplets on the fluid's free surface. Several SPH-based fluid solvers exist including Weakly compressible SPH (WCSPH) [12], Predictive-Corrective Incompressible SPH (PCISPH) [13], and Divergence-Free SPH (DFSPH) [14]. Among them, DFSPH is arguably the most advanced fluid solver that can guarantee the incompressibility and divergence-free conditions of the fluid.

Multiphase Fluid Simulation: Multiphase fluid simulation can simulate a mixture of several miscible or non-miscible components, such as is the case of bone cement. In more detail, multiphase simulations can handle different material components, like a mixture of water and sand (for cement) or different states of the same material, such as water and bubbles. Current multiphase flow simulation research covers bubble simulation [15], [16], phase transition [17], and improving numerical accuracy [18]–[20]. Commonly used multiphase fluid simulation methods include two-fluid models [21], suspension models [22], and mixture models [18]. Among them, the mixture model has received much attention recently. In the mixture model, the volume fraction is used to represent the proportion of different phases at the same sampling position. The overall discretization method uses SPH; the physical field of the fluid is calculated using multiphase fluid dynamics. For more details on SPH and multiphase simulation methods, we refer the interested reader to a recent survey [11].

III. Multiphase non-Newtonian fluid simulation for bone cement flow

The use of bone cement involves two processes: modulation and injection. During *modulation*, two substances – organic solvent and solute – are mixed in different proportions, which leads to varying flow performance during the *injection* phase. The mixed fluid is a non-Newtonian fluid with viscoelastic shear thinning, and polymerization reactions will change its physical properties. The fluid polymerization period can be further split into four stages: coarse sand, drawing, clumping, and hardening. In this paper, we model the fluid based on an implicit mixture model and the polymer conformation tensor method, so as to simulate the dynamic modulation process and the coarse sand flow. The other stages remain as future work.

Previous work [20] assumes that the effect of the mixture on the phases is constant. However, this is not true in some solutions that react. We extend this to the dynamic setting using a bonding effect network (Section III-B) in our algorithm (SectionIII-C). Before doing that, we continue by describing the relevant basics of SPH methods (Section III-A).

A. SPH-based fluid simulation

The SPH method discretizes the continuous fluid medium into independent particles. SPH can be understood as a discretization method for spatial fields and spatial differential operations. The physical field information in space (e.g., fluid density, mass, velocity, pressure) is defined on SPH particles. SPH determines the state information of each particle at the next time step based on the contribution of neighbor particles,

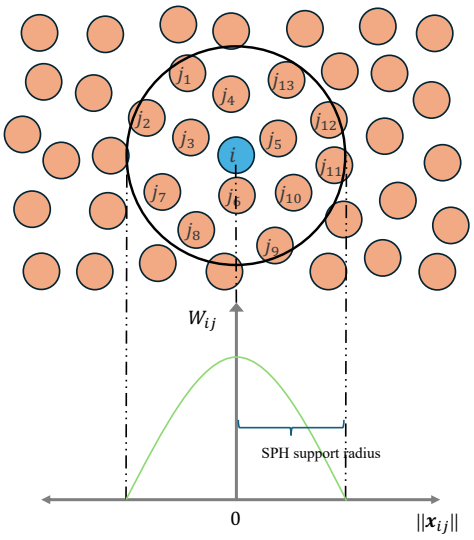

Fig. 3. SPH particle samples. Here, j_s represents the neighbors of particle i, and the curve denotes the Gaussian-like kernel function. When two particles become close, W_{ij} will have a larger value, and when two particles are out of range, W_{ij} will vanish.

weighted by a kernel function (Fig. 3). Specifically, a physical field $\mathbf{A}_i$ (sampled at particle i) is estimated as

$$\mathbf{A}_i = \sum_{j \in N(i)} \frac{m_j}{\rho_j} \mathbf{A}_j W_{ij}, \tag{1}$$

where $N(i)$ is the neighborhood of i that affects that particle, m denotes the particle mass, ρ is the particle density, and W is a Gaussian-like (*e.g.*, cubic spline) kernel function.

Estimating the gradient, divergence, and Laplacian of field $\mathbf{A}$ using the SPH standard discretization can be done as follows

$$\begin{aligned} \nabla \mathbf{A}_i &= \sum_{j \in N(i)} \frac{m_j}{\rho_j} \mathbf{A}_j \otimes \nabla W_{ij}, \\ \nabla \cdot \mathbf{A}_i &= \sum_{j \in N(i)} \frac{m_j}{\rho_j} \mathbf{A}_j \nabla W_{ij}, \\ \nabla^2 \mathbf{A}_i &= \sum_{j \in N(i)} \frac{m_j}{\rho_j} \mathbf{A}_j \nabla^2 W_{ij}, \end{aligned} \tag{2}$$

where $\mathbf{a} \otimes \mathbf{b} = \mathbf{a}\mathbf{b}^T$.

B. Implicit mixture model with improved phase transfer

Implicit Mixture Model: The mixture model uses the volume fraction scheme (Fig. 4) to represent the concentration of each phase and calculates the physical parameters at the phase level and the mixture level using multiphase fluid dynamics.

The sum of the phase volume fractions α_k, for all k existing phases of a particle i, is normalized as

$$\sum_k \alpha_{i,k} = 1. \tag{3}$$

where subscript i, k denotes phase k of particle i.

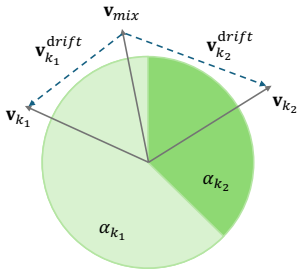

Fig. 4. Example of volume fraction scheme in a mixture model with a two-phase flow (phases are indicated by colors).

The velocity field at the mixture level is reconstructed from the phase-level velocity fields $\mathbf{v}_k$ via

$$\mathbf{v}_{i,\text{mix}} = \sum_k \alpha_{i,k} \mathbf{v}_{i,k}. \tag{4}$$

The density of the mixture particle is computed as

$$\rho_{i,\text{mix}} = \sum_k \alpha_{i,k} \rho_k^0, \tag{5}$$

where ρ_k^0 is the rest density of phase k.

The velocity field at the mixture level $\mathbf{v}_{\text{mix}}$ is used to represent the actual fluid motion, which depends on the calculation of the physical field at the phase level. Here, we use the implicit mixture model [20], where an implicit reconstruction method between mixture level and phase level was derived to achieve higher numerical accuracy. This model considers the effects of gravity, pressure, and viscous forces. The gravity $\mathbf{g}$ belongs to the volume force and is applied equally to each phase. Pressure and viscous forces are computed as

$$\frac{D\mathbf{v}_{i,k}^p}{Dt} = \frac{\mathbf{M}_{i,\text{mix}}^p}{\rho_{i,\text{mix}}} \left(C_d + (1 - C_d) \frac{\rho_{i,\text{mix}}}{\rho_k^0} \right), \tag{6}$$

$$\frac{D\mathbf{v}_{i,k}^\nu}{Dt} = C_d \frac{\mathbf{M}_{i,\text{mix}}^\nu}{\rho_{i,\text{mix}}} + (1 - C_d) \frac{\mathbf{M}_{i,k}^\nu}{\alpha_{i,k} \rho_k^0}, \tag{7}$$

where $\frac{D\mathbf{v}_k}{Dt}$ denotes the acceleration associated with different forces; superscripts p and ν denote pressure and viscosity, respectively; $\mathbf{M}$ represents the momentum source; and $C_d \in [0, 1]$ is the model parameter derived from the implicit mixture model, used to adjust the degree of influence of the mixture on each phase.

Improved Phase Transfer: The phase transfer in the mixture model mainly involves two factors: interphase drag force and diffusion. The calculation of drag force depends on the drift velocity of the phase, which is defined as

$$\mathbf{v}_{i,k}^{\text{drift}} = \mathbf{v}_{i,k} - \mathbf{v}_{i,\text{mix}}. \tag{8}$$

The change of phase fraction due to the two factors is given by

$$\begin{aligned} \frac{D\alpha_{i,k}}{Dt} &= -\sum_{j \in N(i)} V_0 (\alpha_{i,k} \mathbf{v}_{i,k}^{\text{drift}} + \alpha_{j,k} \mathbf{v}_{j,k}^{\text{drift}}) \nabla \cdot W_{ij} \\ \nabla^2 \alpha_{i,k} &= C_f \sum_{j \in N(i)} (\alpha_{i,k} - \alpha_{j,k}) \frac{\mathbf{x}_{ij} \cdot \nabla W_{ij}}{\|\mathbf{x}_{ij}\|^2 + \epsilon}, \end{aligned} \tag{9}$$

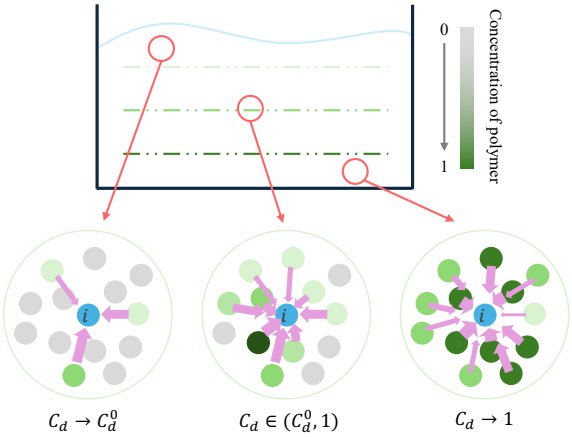

Fig. 5. Our bonding effect network used to model the coupling of phases in an inhomogeneous solution where reactions occur. Using the regions of three concentrations as an example, a greener particle color indicates a higher polymer phase fraction. The arrows indicate the blocking effect of the neighbor on the phase transfer of the target particle i. Thicker arrows indicate a stronger blocking effect.

where C_f is the diffusion coefficient; V_0 denotes the rest volume of a particle; $\mathbf{x}_{ij} = \mathbf{x}_i - \mathbf{x}_j$; $\mathbf{x}$ is the position of the particle; and ϵ is a small regularization constant.

In the implicit mixture model, C_d is used to adjust the degree of influence of the mixture on the phase: when $C_d = 0$, the phase is completely unaffected by the mixture; when $C_d = 1$, the phase is completely controlled by the mixture. In the physical field, the influence of the mixture on the phase is understood as the relationship between the velocity field of the mixture level and the phase level. When the phase velocity field completely follows the mixture, the phase does not separate, which affects phase transport. The original implicit mixture model [20] sets C_d as a constant, indicating that the effect of the mixture on the phase is constant. However, this is not true in some solutions that react. Hence, a mechanism is needed to compute the effect of the solute concentration on the phase transfer.

Calculating the exact intermolecular combination between two molecules can lead to a large overhead. To simplify this computation, we propose to use a *bonding effect network* (see Fig. 5). Specifically, we change the C_d value of the multiphase particle dynamically according to the solute concentration. For one mixture, a basic C_d^0 value is set; we next estimate the current dynamic C_d by the SPH method. We focus on two-phase fluids, where α_{k_1} denotes the liquid phase and α_{k_2} denotes the polymer phase. As such, we have

$$C_d = C_d^0 + (1 - C_d^0) \sum_{j \neq i} V_0 \alpha_{j,k_2} W_{ij}. \tag{10}$$

When the solute concentration around a particle is high, $C_d \to 1$. This will block the phase transfer to simulate the case of phase coupling.

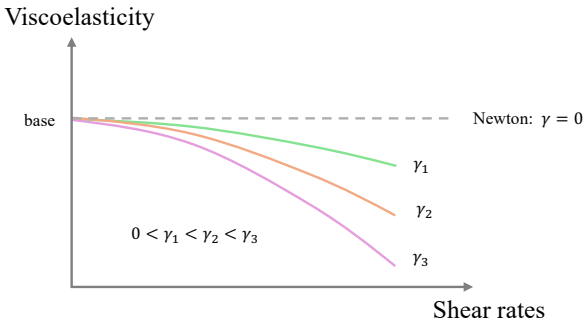

Fig. 6. The shear thinning curve of our model. The viscoelasticity of shear thinning fluid decreases as the shear rate increases. In our model, the larger the value of γ, the stronger the shear thinning effect.

C. Polymer conformation tensor method in the mixture model

The conformation tensor is a tool for describing the material distribution in solutions [23], both for Newtonian and non-Newtonian fluids. The classical configuration update formula for the conformation tensor $\mathbf{U}$ (a 3×3 matrix in the 3D case) is

$$\frac{D\mathbf{U}}{Dt} = \mathbf{U}\nabla\mathbf{v} + (\nabla\mathbf{v})^T\mathbf{U} - \frac{1}{\lambda}(\mathbf{U} - \mathbf{I}), \tag{11}$$

where λ denotes the relaxation time used to describe the fluid viscoelasticity. However, this model can only describe Newtonian fluids; the viscoelasticity of non-Newtonian fluids has a nonlinear relationship with the shear rate. To model this, we use an alternative model given by

$$\frac{D\mathbf{U}}{Dt} = \mathbf{U}\nabla\mathbf{v} + (\nabla\mathbf{v})^T\mathbf{U} - \frac{1}{\lambda}(\mathbf{U} - \mathbf{I}) - \gamma(\mathbf{U} - \mathbf{I})\mathbf{U}, \tag{12}$$

where $\gamma(\mathbf{U} - \mathbf{I})\mathbf{U}$ is a non-linear term that can model shear thinning; and $\gamma \in [0, 1]$ is the thinning factor. A larger value of γ contributes to a stronger thinning effect (Fig. 6).

The mixture-level stress based on the conformation tensor is defined as

$$\tau_{i,\text{mix}} = c\eta_s(\mathbf{U}_i - \mathbf{I}), \tag{13}$$

where c denotes the polymer concentration of the solution, which is equal to α_{k_2} in our multiphase framework; and η_s denotes the viscosity of the solution. We use the symmetric formulation of SPH [24] to calculate the stress force as

$$\frac{1}{\rho_{i,\text{mix}}}\nabla \cdot \tau_{i,\text{mix}} = \sum_{j \in N(i)} \left(\frac{\tau_{i,\text{mix}}}{\rho_{i,\text{mix}}^2} + \frac{\tau_{j,\text{mix}}}{\rho_{j,\text{mix}}^2} \right) \nabla W_{ij}. \tag{14}$$

The conformation tensor method does not define the stress calculation for each phase, and the multiphase framework requires reconstructing the mixture-level velocity from the phase-level velocity. Based on the normalization condition $\tau_{\text{mix}} = \sum_k \tau_k$, we obtain

$$\tau_{i,k} = \alpha_{i,k}\tau_{i,\text{mix}}. \tag{15}$$

In this way, the phase velocity can be updated according to the mixture-level stress as

$$\frac{D\mathbf{v}_{i,k}^{\text{visc}}}{Dt} = \frac{\nabla \cdot \tau_{i,k}}{\alpha_{i,k}\rho_k^0}, \tag{16}$$

Algorithm 1 Bone cement simulation algorithm.

a) Prepare:
1. Modeling bone with different poriness
2. Set injection direction, speed and position
3. Import the particle models and initialize the solver parameters: before the solver loop step, set $\mathbf{U}_i \leftarrow \mathbf{I}$ for all particle i and initialize the neighbors $N(i)$

b) Bone cement modeling and motion solution:

1. Pressure computation
- compute div-free force $\mathbf{M}^p_{i,\text{mix}}$ using **VFSPH**
- update phase velocity $\mathbf{v}_{i,k}$ ▷ Eq. 6
- update mixture velocity $\mathbf{v}_{i,\text{mix}}$ ▷ Eq. 4

2. Advect
- update phase velocity using $\mathbf{v}_{i,k} \leftarrow \mathbf{v}_{i,k} + \mathbf{g}\Delta t$
- update mixture velocity $\mathbf{v}_{i,\text{mix}}$ ▷ Eq. 4

3. Viscoelasticity computation
- update C_{di} ▷ Eq. 10
- update conformation tensor $\mathbf{U}_i$ ▷ Eq. 11
- compute viscoelastic force ▷ Eq. 13, 14
- update phase velocity $\mathbf{v}_{i,k}$ ▷ Eq. 16
- update mixture velocity $\mathbf{v}_{i,\text{mix}}$ ▷ Eq. 4

4. Final step
- update phase volume fraction $\alpha_{i,k}$ ▷ Eq. 9
- update phase drift velocity $\mathbf{v}^{\text{drift}}_{i,k}$ ▷ Eq. 8
- update particle position using $\mathbf{x}_i \leftarrow \mathbf{x}_i + \mathbf{v}_{i,\text{mix}}\Delta t$
- update neighbors $N(i)$
- store the point cloud $\mathbf{x}_i$ according to the output frame rate

–End Sim Loop–

c) Render: From the simulated point clouds $\{\mathbf{x}_i\}$, we finally reconstruct and render the fluid surface using e.g. Houdini.

where $\frac{D\mathbf{v}_k^{\text{visc}}}{Dt}$ represents the acceleration associated with the viscoelastic force.

Algorithm 1 outlines our end-to-end simulation and visualization method called IMM-CT (implicit mixture model with conformation tensor). At the start, some preparatory work is required, including bone modeling, setting the scene and model parameters (step a). When initializing the model parameters, $\mathbf{U}$ is set to $\mathbf{I}$, and a uniform grid is used to update the neighbors $N(i)$ of each particle i. Then, step b solves the dynamic parameters of the multiphase fluid according to the initial input, including pressure, gravity, viscoelastic forces and implements phase transport. Finally the fluid surface is reconstructed using 3D utilities and rendered.

IV. Experiments

We tested our method by simulating various modulation and mixing/injection processes of bone cement. In the following experiments, we refer to the parameters of our method given in Tab. I. We designed two sets of experiments to verify the advantages of our model, as described next.

Modulation mixing: We set up three sets of mixing scenarios with different viscosity ratios. The base viscosity (i.e., solvent viscosity) was set to $0.01\ Pa \cdot s$. The experiment details the stability and performance of the mixing process of different schemes under different viscosity ratios of substances. Figure 7 shows the setup of the experiment. Figure 8 visually compares results obtained by our method (IMM-CT) with two other schemes (DFSPH and IMM). Figure 9 shows the maximum acceptable time step versus viscosity ratio for the tested schemes. It reveals that our IMM-CT scheme has advantages in both stability and performance.

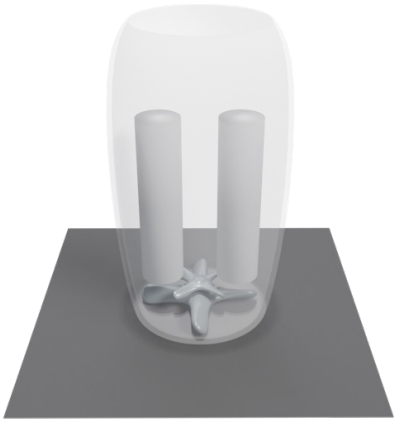

Fig. 7. Modulation mixing scene. The two cylinders in the container are the two phases to be mixed by the high-speed rotating fan below them.

Injection: We chose vertebral fillings, which are common in surgery, as a demonstration. We model the bone interior as a porous material with different local porosities (Fig. 10). We use Blender to model the porous structure, first endow the Mesh object with volume and adjust the local density, and then convert the volume into mesh. We next injected different concentrations and dosages of bone cement into the bone to observe the filling process. This experiment aims to reflect the surgical results caused by different proportions and dosages as shown next in Fig. 11. Different modulation ratios lead to different fluidity of the cement. In the scenario of $0.8 : 0.2$ (first two rows in Fig. 11), the purpose of filling can be quickly achieved, but it is also easy to overflow. The ratio of $0.45 : 0.55$ (second two rows in Fig. 11) shows good performance, and the ratio of $0.15 : 0.85$ leads (third two rows in Fig. 11) to too viscous fluid, so that the fluidity is insufficient, and the filling cannot be completed, so there is no target image.

It is worth noting that in our work the polymer phase has a viscosity of 8 $Pa \cdot s$. In practice, viscosity can be set according to the properties of the products, so different mixing proportion will follow. In addition to the effect of the modulation ratio on the dispersion of the fluid, the filling situation is also affected by the injection speed and injection direction, among other factors. Although we have not given the corresponding demonstration, these experiments are completely feasible. Due to the reason of rendering, the filling situation inside the bone

TABLE I
Model parameters

Parameter	Meaning	Range
C_f	diffusion coefficient	[0, 1]
C_d^0	rest drag coefficient	[0, 1]
γ	phase volume fraction threshold	[0, 1]
η_s	rest viscosity of solution	(0, 15)
λ	relaxation time	(0, 1)

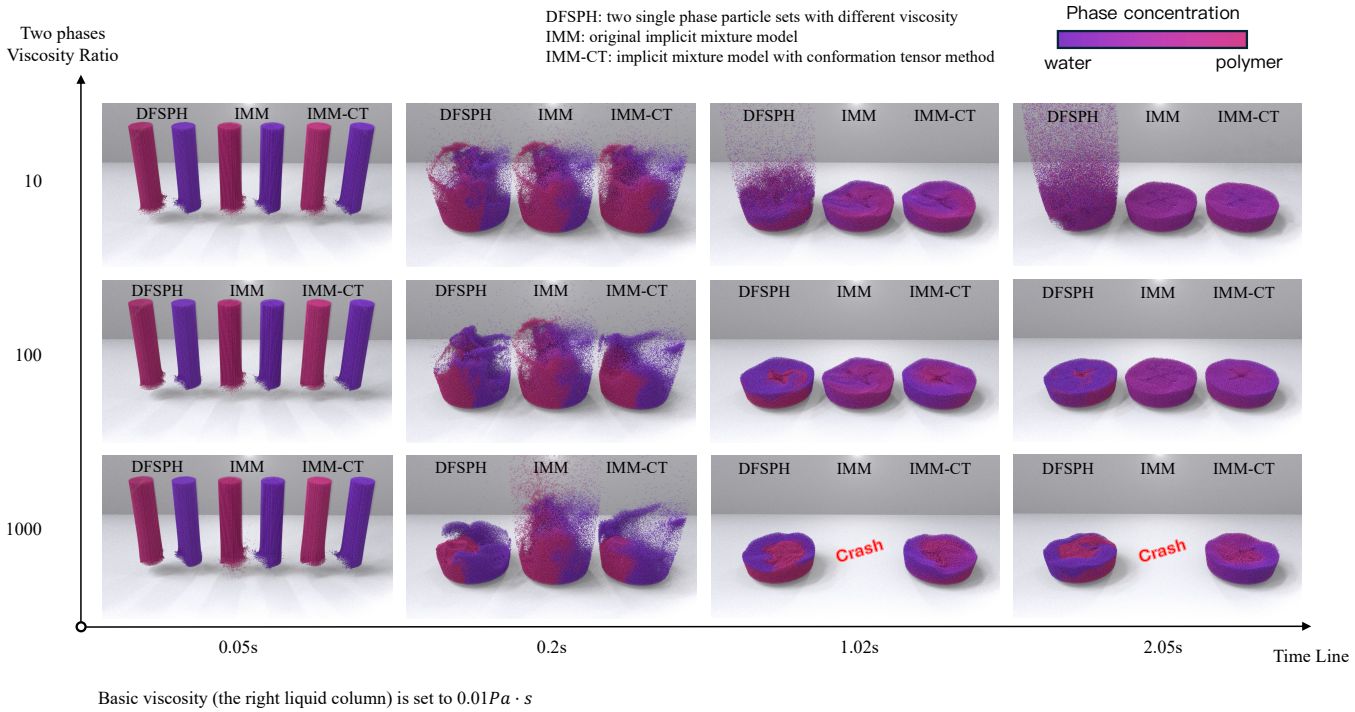

Fig. 8. Three schemes (DFSPH, IMM, and IMM-CT) are used to mix fluids with three different viscosity ratios to compare stability and performance. In the 1:10 scenario, DFSPH shows instability when the fluid is stirred at high speed. In the 1:100 scenario, all the three methods can run stably, but DFSPH cannot obtain a uniform mixed state. In the 1:1000 scenario, DFSPH still can't evenly mix and IMM fails to run stably with an acceptable time step, the simulation collapsed at high speed of stirring. Our method (IMM-CT) runs stably in all three scenarios.

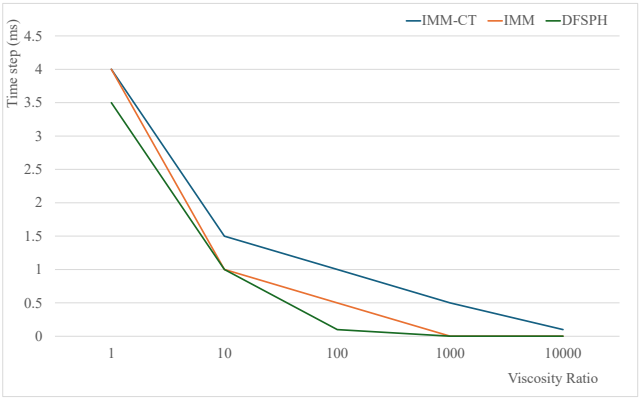

Fig. 9. Comparison of the maximum acceptable time step for three schemes at different viscosity ratios. We define the viscosity ratio as the solute viscosity over the solvent viscosity, and the unit of viscosity is $Pa \cdot s$. Our method (IMM-CT) maintains the advantage in all cases. For viscosity ratios below 0.001, both IMM and DFSPH fail to stabilize the simulation.

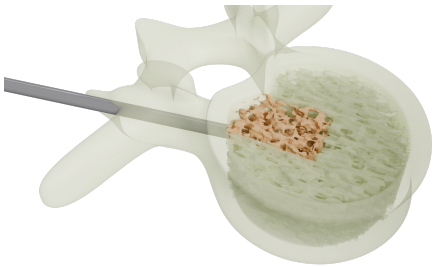

Fig. 10. Bone cement injection scene. The long silver tube is an injecting syringe. The bone interior is modeled as a porous structure with different regions having different sparsities. Darker orange regions in the figure are the sparser regions, which are used to simulate osteoporosis.

cement may not be fully presented, resulting in visual artifacts of the area vacancy on the image (Fig. 11). We provided renders from two perspectives for each set of experiments to compensate for the missing filling area caused by rendering.

V. Conclusion

We have presented a multiphase non-Newtonian fluid simulation method based on the conception tensor method, capable of covering simulations of material mixing with a wide range of viscosity ratios at acceptable time steps, and combined with porous media modeling. Our method targets simulating the full flow of bone cement injection efficiently and effectively, thereby helping practitioners to experiment with different simulation parameters in a cost-effective way. Compared with other existing methods, our model has advantages in performance and stability.

Future work includes extending the model to support solidification and other stages in the flow phase of bone cement. An equally interesting direction is to incorporate the treatment of tension and capillary forces which plain an important role in real materials.

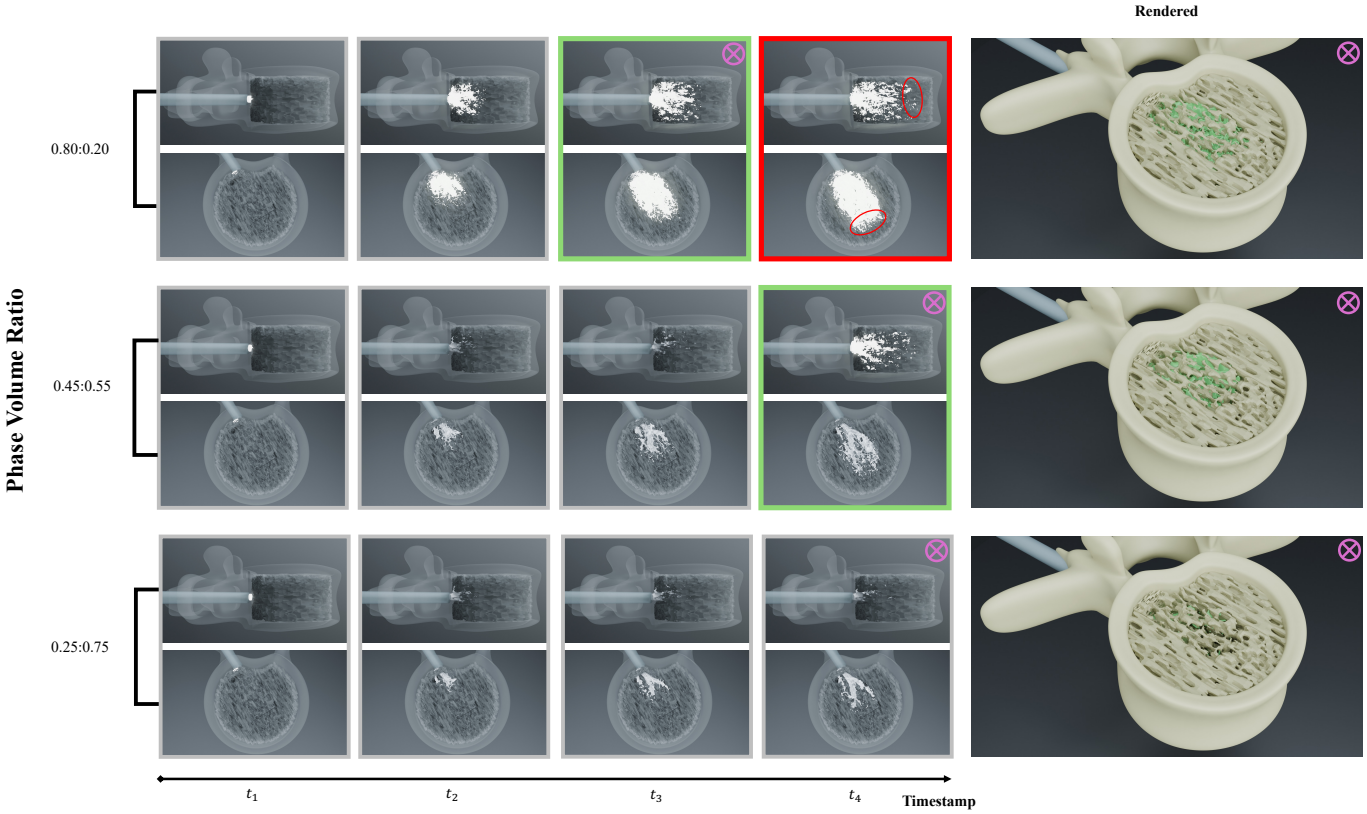

Fig. 11. Three scenarios of bone cement injection with different proportions. The volume ratio of solvent to solute is shown on the left side of the figure. Each row shows a few frames from the injection process; each column represents the same timestamp. Gray boxes around the images indicate insufficient dispersion; green boxes indicate appropriate dispersion; red boxes indicate that overflow occurs. The right column shows the top view at the appropriate injection volume.

VI. Acknowledgements

This research was supported by the National Natural Science Foundation of China (No. 62306032), the National Key Research and Development Program of China (No. 2022ZD0118001), the Guangdong Basic and Applied Basic Research Foundation (No. 2022A1515110350), and the Interdisciplinary Research Project for Young Teachers of USTB (No. FRF-IDRY-22-025). The computing work is partly supported by the MAGICOM Platform of Beijing Advanced Innovation Center for Materials Genome Engineering.

References

[1] R. Vaishya, M. Chauhan, and A. Vaish, "Bone cement," *Journal of clinical orthopaedics and trauma*, vol. 4, no. 4, pp. 157–163, 2013.

[2] S. Saha and S. Pal, "Mechanical properties of bone cement: a review," *Journal of biomedical materials research*, vol. 18, no. 4, pp. 435–462, 1984.

[3] J. Charnley, "Anchorage of the femoral head prosthesis to the shaft of the femur," *The Journal of Bone & Joint Surgery British Volume*, vol. 42, no. 1, pp. 28–30, 1960.

[4] J. Nicholson, S. Hawkins, and E. Wasson, "A study of the structure of zinc polycarboxylate dental cements," *Journal of Materials Science: Materials in Medicine*, vol. 4, pp. 32–35, 1993.

[5] A. D. Wilson and B. Kent, "The glass-ionomer cement, a new translucent dental filling material," *Journal of Applied Chemistry and Biotechnology*, vol. 21, no. 11, pp. 313–313, 1971.

[6] S. K. Sidhu and J. W. Nicholson, "A review of glass-ionomer cements for clinical dentistry," *Journal of functional biomaterials*, vol. 7, no. 3, p. 16, 2016.

[7] E. Truumees, A. Hilibrand, and A. R. Vaccaro, "Percutaneous vertebral augmentation," *The Spine Journal*, vol. 4, no. 2, pp. 218–229, 2004.

[8] P. R. Ebeling, K. Akesson, D. C. Bauer, R. Buchbinder, R. Eastell, H. A. Fink, L. Giangregorio, N. Guanabens, D. Kado, D. Kallmes *et al.*, "The efficacy and safety of vertebral augmentation: a second asbmr task force report," *Journal of Bone and Mineral Research*, vol. 34, no. 1, pp. 3–21, 2019.

[9] S. Breusch, H. Malchau, M. Clarius, C. Heisel, and S. J. Breusch, "Pulmonary embolism in cemented total hip arthroplasty," *The Well-Cemented Total Hip Arthroplasty: Theory and Practice*, pp. 320–331, 2005.

[10] N. Moussazadeh, D. G. Rubin, L. McLaughlin, E. Lis, M. H. Bilsky, and I. Laufer, "Short-segment percutaneous pedicle screw fixation with cement augmentation for tumor-induced spinal instability," *The Spine Journal*, vol. 15, no. 7, pp. 1609–1617, 2015.

[11] X. Wang, Y. Xu, S. Liu, B. Ren, J. Kosinka, A. C. Telea, J. Wang, C. Song, J. Chang, C. Li *et al.*, "Physics-based fluid simulation in computer graphics: Survey, research trends, and challenges," *Computational Visual Media*, pp. 1–56, 2024.

[12] M. Becker and M. Teschner, "Weakly compressible sph for free surface flows," in *Proceedings of the 2007 ACM SIGGRAPH/Eurographics symposium on Computer animation*, 2007, pp. 209–217.

[13] B. Solenthaler and R. Pajarola, "Predictive-corrective incompressible sph," in *ACM SIGGRAPH 2009 papers*, 2009, pp. 1–6.

[14] J. Bender and D. Koschier, "Divergence-free smoothed particle hydrodynamics," in *Proceedings of the 14th ACM SIGGRAPH/Eurographics symposium on computer animation*, 2015, pp. 147–155.

[15] V. Mihalef, D. Metaxas, and M. Sussman, "Simulation of two-phase

flow with sub-scale droplet and bubble effects," in *Computer Graphics Forum*, vol. 28, no. 2. Wiley Online Library, 2009, pp. 229–238.
[16] B. Ren, Y. Jiang, C. Li, and M. C. Lin, "A simple approach for bubble modelling from multiphase fluid simulation," *Computational Visual Media*, vol. 1, pp. 171–181, 2015.
[17] Z. Tu, C. Li, Z. Zhao, L. Liu, C. Wang, C. Wang, and H. Qin, "A unified mpm framework supporting phase-field models and elastic-viscoplastic phase transition," *ACM Transactions on Graphics*, vol. 43, no. 2, pp. 1–19, 2024.
[18] B. Ren, C. Li, X. Yan, M. C. Lin, J. Bonet, and S.-M. Hu, "Multiple-fluid sph simulation using a mixture model," *ACM Transactions on Graphics (TOG)*, vol. 33, no. 5, pp. 1–11, 2014.
[19] Y. Jiang and Y. Lan, "A dynamic mixture model for non-equilibrium multiphase fluids," in *Computer Graphics Forum*, vol. 40, no. 7. Wiley Online Library, 2021, pp. 85–95.
[20] Y. Xu, X. Wang, J. Wang, C. Song, T. Wang, Y. Zhang, J. Chang, J. J. Zhang, J. Kosinka, A. Telea *et al.*, "An implicitly stable mixture model for dynamic multi-fluid simulations," in *SIGGRAPH Asia 2023 Conference Papers*, 2023, pp. 1–11.
[21] M. Ishii, "Two-fluid model for two-phase flow," *Multiphase science and technology*, vol. 5, no. 1-4, 1990.
[22] M. Wyart and M. E. Cates, "Discontinuous shear thickening without inertia in dense non-brownian suspensions," *Physical review letters*, vol. 112, no. 9, p. 098302, 2014.
[23] A. Bejan, "The constructal law of organization in nature: tree-shaped flows and body size," *Journal of Experimental Biology*, vol. 208, no. 9, pp. 1677–1686, 2005.
[24] J. J. Monaghan, "Smoothed particle hydrodynamics," *Reports on progress in physics*, vol. 68, no. 8, p. 1703, 2005.